

# Exchange interactions and the origin of the spin gap in $\text{Sr}_2\text{ScOsO}_6$

A. E. Taylor,<sup>1,\*</sup> R. Morrow,<sup>2</sup> R. S. Fishman,<sup>3</sup> S. Calder,<sup>1</sup> A.I. Kolesnikov,<sup>4</sup>  
M. D. Lumsden,<sup>1</sup> P. M. Woodward,<sup>2</sup> and A. D. Christianson<sup>1,5</sup>

<sup>1</sup>*Quantum Condensed Matter Division, Oak Ridge National Laboratory, Oak Ridge, Tennessee 37831, USA*

<sup>2</sup>*Department of Chemistry, The Ohio State University, Columbus, Ohio 43210-1185, USA*

<sup>3</sup>*Materials Science and Technology Division, Oak Ridge National Laboratory, Oak Ridge, Tennessee 37831, USA*

<sup>4</sup>*Chemical and Engineering Materials Division, Oak Ridge National Laboratory, Oak Ridge, Tennessee 37831, USA*

<sup>5</sup>*Department of Physics and Astronomy, The University of Tennessee, Knoxville, TN 37996, USA*

The double perovskite  $\text{Sr}_2\text{ScOsO}_6$  hosts  $5d^3$   $\text{Os}^{5+}$  ions that are nominally orbitally-quenched, however, neutron scattering experiments reveal a large gap in the magnetic excitation spectrum of  $\text{Sr}_2\text{ScOsO}_6$  below  $T_N$ . Spin-orbit coupling induced exchange anisotropy is identified as the likely origin of the gap, and the system is modeled with a Heisenberg Hamiltonian including exchange anisotropy. Limited experimental constraints allow determination of the isotropic exchange parameters, independent of the origin of the gap, and the resulting spin-wave spectrum reproduces the observed low-temperature data. The results demonstrate that spin-orbit coupling is manifest in the physical properties of  $\text{Sr}_2\text{ScOsO}_6$ , and similar  $4d^3$  and  $5d^3$  systems.

Attempts to find  $J_{\text{eff}} = \frac{1}{2}$  states [1–8] and the exactly-solvable Kitaev Hamiltonian [9–11] in iridate materials have recently attracted a great deal of interest. Robust  $JJ$ -coupled states are attractive since they are well-defined quantum states, readily allowing materials' properties to be modeled. These models, however, largely rely on ideal geometries and the particular  $\text{Ir}^{4+}$   $5d^5$  electronic configuration; most materials lie outside of this ideal [12]. The role of SOC in  $4d$  and  $5d$  transition metal oxides is relatively poorly understood outside of the  $LS$  and  $JJ$  coupling limits.

The need to understand the intermediate SOC regime is typified by the diverse range of properties found in double perovskites (DPs) containing  $4d$  and  $5d$  ions, including high-temperature half-metallic ferrimagnetism [13, 14], structurally selective magnetic states [15–17], complex geometric frustration [18–23], and Mott insulating ferromagnetism [24, 25]. Whilst this complex array of ground states has generated a great deal of interest, the interaction mechanisms controlling many of them remain undetermined.

For DP materials hosting  $4d^3$  and  $5d^3$  ions, there exists dispute between different theories describing the  $d^3$  state, the interactions and the role of SOC [26, 27]. To first order,  $d^3$  ions in an octahedral environment are expected to be orbitally quenched, Fig. 1(a) [21, 28], yet there is mounting evidence that SOC has considerable influence [18, 23, 29–31]. This has been demonstrated experimentally by the presence of gaps of  $\sim 2$ – $18$  meV in the magnetic excitation spectra of polycrystalline  $\text{Ba}_2\text{YRuO}_6$ ,  $\text{La}_2\text{NaRuO}_6$  and  $\text{Ba}_2\text{YO}_6$ , observed via inelastic neutron scattering (INS) [21, 23, 29]. With the origin of a gap relying on anisotropy, the presence of such large gaps, on the same energy scale as the  $T_N$ s, indicates the existence of significant magnetic anisotropy. Although SOC has been noted as the origin [23, 29], the underlying mechanism by which SOC acts to produce the gap remains an open question.

Aside from the fundamental interest in the influence of SOC, it is vital to determine the interactions in  $5d^3$  DPs in order to understand the exceptionally high  $T_C = 725$  K discovered in  $\text{Sr}_2\text{CrOsO}_6$  [32, 33]. The  $5d^3$  Os ions participate in the magnetism and their role cannot be neglected [34]. However, with no single crystals available, the high magnetic energy scale and the interplay between two magnetic ions both inhibit the determination of the magnetic interactions.

We have identified  $\text{Sr}_2\text{ScOsO}_6$  as a model system for investigating the role of the  $5d^3$  magnetic interactions in a high transition temperature material. It is the single-magnetic-ion analogue of  $\text{Sr}_2\text{CrOsO}_6$  — it therefore has large spatial separation between magnetic ions, which results in correspondingly lower energy scales. However it still hosts a remarkably high  $T_N$  (92 K) for a single-magnetic-ion DP [31, 35, 36], and therefore allows the magnetic interactions resulting solely from  $5d^3$   $\text{Os}^{5+}$  to be probed.

We present the INS spectrum of  $\text{Sr}_2\text{ScOsO}_6$  measured on a polycrystalline sample, and find a large spin gap below  $T_N$ . A Heisenberg Hamiltonian with anisotropic exchange terms is considered. Over a large parameter space, limited experimental constraints on the Hamiltonian enable the extraction of the nearest neighbor (NN),  $\mathcal{J}_1$ , and next nearest neighbor (NNN),  $\mathcal{J}_2$ , exchange terms. The success of the model, along with further physical arguments, indicate that anisotropic exchange is the primary candidate for the microscopic origin of the gap. Independent of the origin of the spin gap, we determine that the isotropic components must lie in the range  $J_1 = -6.5$  to  $-8.5$  meV and  $J_2 = -3.4$  to  $-4.1$  meV in order to reproduce the data. These results demonstrate that SOC within the  $5d^3$  manifold is a key ingredient for the collective behavior realized in  $\text{Sr}_2\text{ScOsO}_6$  and related  $4d^3$  and  $5d^3$  systems.

A 16.5 g polycrystalline sample of  $\text{Sr}_2\text{ScOsO}_6$  was used for INS experiments on SEQUOIA at the Spallation Neu-

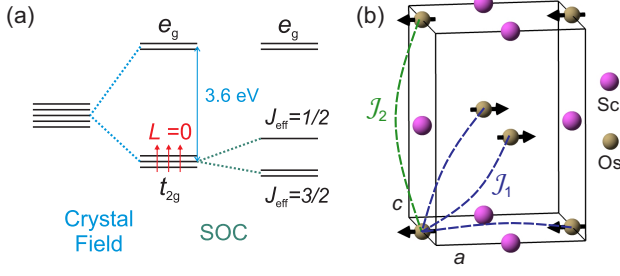


Figure 1. (a) Schematic of the energy levels for  $\text{Os}^{5+}$  in an octahedral environment.  $t_{2g}$ - $e_g$  splitting of 3.6 eV determined by x-ray absorption spectroscopy [37]. In the strong SOC limit the  $t_{2g}$  level can be further split into  $J_{\text{eff}} = \frac{1}{2}$  and  $\frac{3}{2}$  levels. Nominally the  $\text{Os}^{5+}$  ion is in the  $LS$  coupling limit and an  $L = 0$  state results. (b)  $\text{Sr}_2\text{ScOsO}_6$  magnetic structure, with moments depicted along  $a$ . One  $P2_1/n$  unit cell is shown, with O and Sr ions omitted for clarity. Dashed lines show examples of the NN ( $\times 12$ )  $J_1$  and NNN ( $\times 6$ )  $J_2$  exchanges, assuming small differences in distance due to the monoclinic distortion are negligible.

tron Source at Oak Ridge National Laboratory [38]. A portion of this sample was used to investigate the structural and magnetic properties as reported in Ref. [31]. Measurements were between 6 K and 115 K, using incident energies,  $E_i$ , of 60 and 120 meV with chopper frequencies of 180 and 300 Hz, respectively. Empty Al-can measurements were subtracted from the data sets presented; raw  $\text{Sr}_2\text{ScOsO}_6$  and empty-can data are shown in the Supplemental Material (SM) [39].

The measured INS spectra at 6, 50, 80 and 95 K are shown in Fig. 2. There is a pronounced change in the spectrum at low neutron momentum transfer ( $Q$ ) upon crossing  $T_N = 92$  K. This behavior is reminiscent of the observed gap development below  $T_N$  in other single magnetic ion  $4d^3$  and  $5d^3$  DPs [21, 23, 29]. The higher  $Q$  scattering, which changes only in intensity with temperature, is identified as phonon scattering.

The detailed  $(Q, E)$ -space structure and temperature dependence of the scattering is presented in Fig. 3. Figure 3(a) demonstrates that intensity is distributed to higher energies at low temperatures, as expected from a gap opening. The peak of the scattering intensity at 6 K is  $\eta = 19(2)$  meV. This compares to previous observations, which have been used as a magnitude estimate for the gap, of  $\eta = 18(2)$  meV in  $\text{Ba}_2\text{YOsO}_6$  ( $T_N=69$  K),  $\eta \approx 5$  meV in  $\text{Ba}_2\text{YRuO}_6$  ( $T_N=36$  K) and  $\eta \approx 2.75$  meV in  $\text{La}_2\text{NaRuO}_6$  ( $T_N=15$  K) [21, 23, 29]. This generally supports a picture of gap-energy scale varying with  $T_N$ . Figure 3(c) presents data that has been corrected for the Bose thermal population factor,  $[1 - \exp(-E/k_B T)]^{-1}$ . The sharp drop in intensity at low  $E$  below  $T_N$  demonstrates the opening of the gap.

Figure 3(d) presents constant- $E$  cuts averaged from 5 to 9 meV. The scattering is centered around the antiferro-

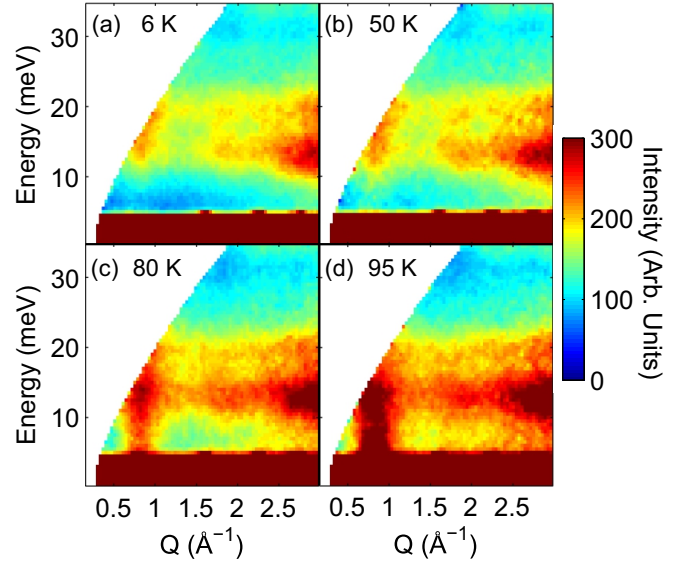


Figure 2. Neutron scattering intensity maps showing the evolution of the scattering from 95 K  $\approx T_N$ , to 80, 50 and 6 K  $< T_N$ , measured with  $E_i = 60$  meV.

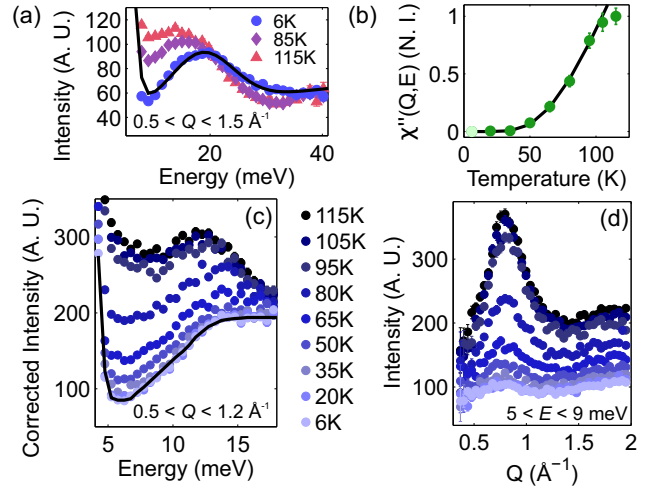


Figure 3. (a) Constant- $Q$  cuts from  $E_i = 120$  meV data. The solid line is the result of fitting Gaussians to the elastic line and to the inelastic magnetic signal at 6 K. A. U. stands for arbitrary units. (b)  $\chi''(T)$  at fixed  $Q$  and  $E$ , with an exponential,  $\chi''(T) \propto \exp(-\Delta/k_B T)$ , fit to the  $T < T_N$  data. N.I. stands for normalized intensity. (c) Constant- $Q$  cuts from  $E_i = 60$  meV data, which have been corrected for the Bose factor. Solid line is a guide to the eye. (d) Constant- $E$  cuts from  $E_i = 60$  meV data. In all panels errorbars are plotted, but are sometimes smaller than the symbols.

magnetic (AFM) ordering wavevector  $|\mathbf{Q}_{(001)}| \approx 0.8 \text{ \AA}^{-1}$ , with some asymmetry in the lineshape resulting from  $|\mathbf{Q}_{(100)/(010)}| \approx 1.1 \text{ \AA}^{-1}$  fluctuations. To track the relative strength of the fluctuations with temperature we extract the dynamic susceptibility,  $\chi''(T)$ , for fixed range  $5 < E < 9$  meV and  $0.5 < Q < 1.2 \text{ \AA}^{-1}$  via the same

method as Ref. [23] (see also SM [39]). The opening of a gap below  $T_N$  is again indicated, Fig. 3(b), by the reduction in  $\chi''(T)$  at low-energy.

To reproduce the data, we investigate a model Heisenberg Hamiltonian. We parametrize the model with isotropic terms, the magnitude of which are decoupled from the physical origin of the spin gap, and exchange anisotropy terms to account for the gap. Unlike isotropic exchange terms, the anisotropic exchange terms only couple to a particular component of spin, e.g.  $S_x$ . We assume that both NN and NNN interactions  $\mathcal{J}_1$  and  $\mathcal{J}_2$ , Fig. 1(b), are anisotropic in spin space. The Heisenberg exchanges are written as

$$\begin{aligned}\mathcal{J}_{1\alpha\beta} &= J_1\delta_{\alpha\beta} + K_1\delta_{\alpha x}\delta_{\beta x} \\ \mathcal{J}_{2\alpha\beta} &= J_2\delta_{\alpha\beta} + K_2\delta_{\alpha x}\delta_{\beta x}.\end{aligned}$$

$J_1$ ,  $J_2$  and  $K_1$ ,  $K_2$  are the magnitudes of isotropic and anisotropic components, respectively, defined such that positive values are ferromagnetic (FM) and negative values are AFM.  $x$  represents the direction of spin alignment, which in crystallographic space is within the  $a$ - $b$  plane [31]. Since the model assumes that all 12 NN, and 6 NNN distances are equivalent, the real-space  $a$ - $b$  plane alignment of the spins does not affect the calculation. The exchange parameters scale inversely with spin,  $s$ . We use the Os moment determined from neutron diffraction,  $m = 1.6(1) \mu_B$  [31], giving  $s = 0.8$  [40].

Obtaining the exchange interactions allows the underlying behavior of a system to be understood, however doing so is non-trivial and previous investigations on similar systems have not achieved this. To accurately reproduce the INS data from  $\text{Sr}_2\text{ScOsO}_6$ , we first determine loose constraints on the parameter space. To achieve this we solve for the four parameters  $J_1$ ,  $J_2$ ,  $K_1$ , and  $K_2$  based on four conditions. First, the ground state of the Os spins is the one depicted in Fig. 1(b). To confirm the ground state, we minimize the classical energy  $\epsilon$  among the 64 different spin configurations with distinct Os spins aligned along the  $\pm x$  directions in layers  $z = 0, c/2, c$ , and  $3c/2$ . Another stipulation for the local stability of the ground state is that the spin-wave frequencies are real throughout the magnetic Brillouin zone.

The second (third) condition is that the the bottom (top) of the spin-wave band is  $\Delta = 12$  meV ( $\Gamma = 40$  meV). The value of  $\Delta$  was selected by inspection of the 6 K data in Fig. 3(c), in which the increasing intensity begins to saturate at  $E \approx 12$  meV. The value of  $\Gamma$  was selected by inspection of broad constant- $Q$  cuts from the  $E_i = 120$  meV data sets (see SM Fig. S2 [39]), designed to capture all magnetic scattering up to high energies, in which 6 K and 115 K cuts converge at 40 meV. We tested alternative values of  $\Delta$  and  $\Gamma$ , and found that these did not reproduce the neutron scattering data, see SM [39]. We note that conditions two and three for  $\Delta$  and  $\Gamma$  are

not independent, and that exchange anisotropies  $K_1$  and  $K_2$  have the same effect on the spin dynamics as a single anisotropy term  $\kappa = 3K_2 - 2K_1$ .

Finally, among parameters that nearly satisfy the first three conditions, we choose those that most closely give the observed  $T_N$  of 92 K. While the conditions for the spin-wave energies  $\Delta$  and  $\Gamma$  are closely satisfied, the mean field transition temperature exceeds the measured  $T_N$  by a factor of two. Since mean field theory typically overestimates the experimental  $T_N$ , and the Curie-Weiss constant for this compound,  $\Theta = -677$  K [31], is also far greater than 92 K, this is not surprising.

The parameters are calculated over a large range of initial  $K_1$  values. For each  $K_1$ , there are only two distinct branches of solutions, one with  $J_1 < 0$  and the other with  $J_1 > 0$ . We find ranges of possible solutions for  $J_1$ ,  $J_2$  and  $K_2$  for each  $K_1$ , even though  $\Delta$  and  $\Gamma$  depend only on the combination  $\kappa = 3K_2 - 2K_1$ , because the problem is under-determined [39]. For both branches, however, the average value for  $\kappa$  is constant over most of the range of  $K_1$  (Fig. S3 [39]). Note that the energy  $\epsilon$  does not simply depend on  $\kappa$ .

Having determined the regions of parameter space which match our minimal constraints, we compare the simulated powder-averaged INS cross sections  $S(Q, E)$  to the low-temperature data, Fig. 4. The comparison tightly constrains the correct solutions out of the large parameter space searched. The branch of solutions with FM  $J_1 > 0$  fail to reproduce the observed data (see Fig. S4[39]). The  $S(Q, E)$  calculated with AFM  $J_1 < 0$ , however, qualitatively reproduce the 6 K data very well, Fig. 4. The comparison between calculation and  $E_i = 60$  meV data in Fig. 4(a) and (b) shows that the data are reproduced in the high-resolution configuration, but also indicates that accessing higher  $E$  and lower  $Q$  is desirable. This requires higher  $E_i$ , hence the equivalent calculation and  $E_i = 120$  meV data are shown in Fig. 4(c) and (d); the data are again very well reproduced. The loss of both experimental resolution and incident neutron flux limits the value of collecting data at higher  $E_i$ .

The simulations presented in Fig. 4 are for parameters  $K_1 = -5.8$  meV,  $J_1 = -7.5$  meV,  $J_2 = -3.95$  meV and  $K_2 = 3.75$  meV, as these are physically reasonable parameters for which  $J_1 > K_1$  and  $J_2 > K_2$ . Unique solutions for  $K_1$  and  $K_2$  cannot be found due to the constraints of modeling a polycrystalline data set, see SM for additional solutions [39], but the values of  $J_1$  and  $J_2$  are stable across the solutions. Therefore, the determined range of values  $J_1 = -6.5$  to  $-8.5$  meV and  $J_2 = -3.4$  to  $-4.1$  meV are a robust description of the experimental data, independent of the origin of the spin gap. The determination that both  $J_1$  and  $J_2$  are AFM has significant implications for modeling the  $\text{Os}^{5+}$  DPs, as we discuss below.

A spin gap emerges due to the moments coupling to a preferred direction within the crystal lattice. In general,

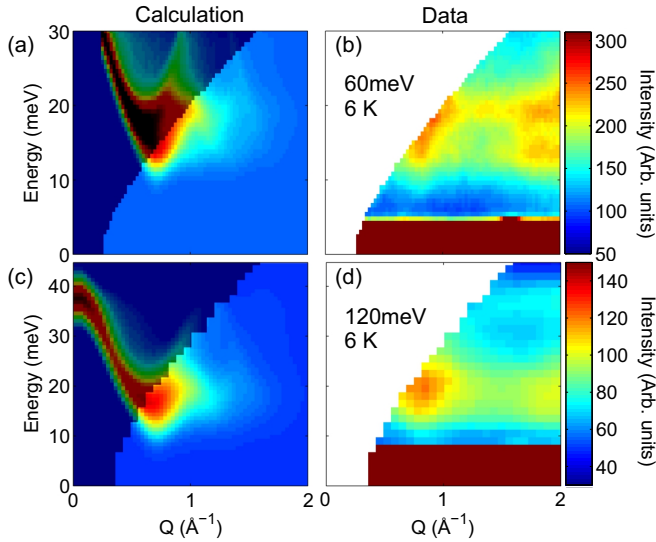


Figure 4. (a) and (c) Simulated spin-wave spectra, from calculated parameters  $K_1 = -5.8$  meV,  $J_1 = -7.5$  meV,  $J_2 = -3.95$  meV and  $K_2 = 3.75$  meV. Modeled using linear spin-wave theory [41], with powder averaging performed by sampling  $10^4$  random points in reciprocal space. Gaussian energy broadening is applied, as an approximation to instrument resolution, using 4 meV ((a)) and 6.8 meV ((c)), estimated from the full width at half maximum of the incoherent part of the elastic line in the data sets. The equivalent data sets collected at  $T = 6$  K with (b)  $E_i = 60$  meV and (d)  $E_i = 120$  meV are shown. The intensity at high  $Q$  in the data is due to phonon scattering, which is not included in the model. The shaded region in the calculations indicates the region of  $(Q, E)$  space which is inaccessible in the experiment.

the possible origins of such behavior in a three dimensional system are Dzyaloshinsky-Moriya (DM) interactions, single-ion anisotropy, and exchange anisotropy, all of which are induced by SOC. There are two observations which favor dismissal of the DM interaction as the origin of the gap: (i) the highly symmetric cubic or close-to-cubic crystal structures in which the gap has been observed [42] and (ii) the type I collinear AFM structure common to several DPs including  $\text{Sr}_2\text{ScOsO}_6$  – two perpendicular DM interactions would be required to produce a gap, but this would favor a non-collinear spin state.

We also expect that single-ion anisotropy is negligible, because it is dramatically suppressed for the orbitally suppressed  $d^3$  configuration, and the 3.6 eV  $t_{2g}$  to  $e_g$  splitting in  $\text{Sr}_2\text{ScOsO}_6$  [37] means that the excited state perturbations are minimal [43]. This is supported by the experimental observation that no gap is observed in  $\text{La}_2\text{NaOsO}_6$  which only displays short-range order, whereas a gap is observed in long-ranged-ordered sister-compound  $\text{La}_2\text{NaRuO}_6$  [29]. A single-ion term, being a local effect, would not be sensitive to short- versus long-range order, and would emerge in the short-range ordered state. Moreover, since the gap opens at  $T_N$  the collective properties of the ordered state appear important. There-

fore, exchange anisotropy is the most-likely explanation for the gap in  $4d^3$  and  $5d^3$  DPs, including  $\text{Sr}_2\text{ScOsO}_6$ . It has previously been discussed as the dominant term over single-ion effects for monoclinic  $5d^3$   $\text{Sr}_2\text{YRuO}_6$  [22]. The presence of a spin gap in  $\text{Ba}_2\text{YRuO}_6$  and  $\text{Ba}_2\text{YOsO}_6$  is surprising, however, since in their ostensibly cubic  $Fm\bar{3}m$  structure anisotropic terms are fourth-order perturbations via the  $t_{2g}$  to  $e_g$  energy gap [43]. As in the single-ion anisotropy case, the large  $t_{2g}$ - $e_g$  splitting would appear to preclude this as an explanation. A small noncubic distortion may allow SOC to enter as a lower order term in  $\text{Ba}_2\text{YOsO}_6$  and  $\text{Ba}_2\text{YRuO}_6$ . However, such a distortion, if present, is outside of the detection limits of current investigations. High resolution studies of the crystal structure have the potential to provide further insight into this issue.

The results presented highlight that SOC must be considered in  $4d^3$  and  $5d^3$  DPs, despite being far from the  $JJ$  coupling limit. The model we present for  $\text{Sr}_2\text{ScOsO}_6$ , including exchange anisotropy, provides an excellent description of the INS data. Previous attempts to model the exchange interactions in  $5d^3$  DPs' using density functional theory have not considered exchange anisotropy [44–46], therefore, further calculations will be essential in light of this work. Calculations for  $\text{Sr}_2\text{ScOsO}_6$  will be constrained by the size of the observed gap and by the determined isotropic parameters, independent of the gap's origin.

The determination that  $J_1$  and  $J_2$  are both AFM in  $\text{Sr}_2\text{ScOsO}_6$  has further implications. Type I AFM order is found in  $\text{Sr}_2\text{ScOsO}_6$ ,  $\text{Sr}_2\text{YRuO}_6$ ,  $\text{Ba}_2\text{YOsO}_6$  and  $\text{Ba}_2\text{YRuO}_6$ , but theoretical calculations for  $\text{Sr}_2\text{YRuO}_6$  found competition between type I and type III AFM order [22]. For an isotropic Heisenberg Hamiltonian, the ground state is type I only if  $J_1$  is AFM whilst  $J_2$  is FM. If both  $J_1$  and  $J_2$  are AFM, then some sort of anisotropy must be included for the ground state to be type I. Our results show that the latter mechanism is the origin of type I order in  $\text{Sr}_2\text{ScOsO}_6$ . Therefore, SOC is essential in determining the magnetic ground state.

As has previously been noted, large Os-O hybridization is an important factor in heightened  $T_N$ s in these DPs [31]. Our results suggest that SOC also acts to enhance  $T_N$  in  $\text{Sr}_2\text{ScOsO}_6$ . By promoting selection of a particular ground state, SOC assists in relieving the inherent frustration of the nearly-face-centered cubic lattice. This notion is supported by the trend in gap size with  $T_N$  across the measured compounds, and by the observation that  $3d$  transition metal DPs have lower  $T_N$ s and usually favor a different, Type II, ground state [47]. This may have significant implications for high transition temperature systems such as  $\text{Sr}_2\text{CrOsO}_6$ .

The authors gratefully acknowledge M. Stone for useful discussions. The research at Oak Ridge National Laboratory's Spallation Neutron Source was supported by the Scientific User Facilities Division, Office of Ba-

sic Energy Sciences, U.S. Department of Energy (DOE). Support for a portion of this research was provided by the Center for Emergent Materials an NSF Materials Research Science and Engineering Center (DMR-1420451). Research by RF sponsored by the DOE, Office of Science, Basic Energy Sciences, Materials Sciences and Engineering Division. This manuscript has been authored by UT-Battelle, LLC under Contract No. DE-AC05-00OR22725 with the U.S. Department of Energy. The United States Government retains and the publisher, by accepting the article for publication, acknowledges that the United States Government retains a non-exclusive, paid-up, irrevocable, world-wide license to publish or reproduce the published form of this manuscript, or allow others to do so, for United States Government purposes. The Department of Energy will provide public access to these results of federally sponsored research in accordance with the DOE Public Access Plan (<http://energy.gov/downloads/doe-public-access-plan>).

---

\* [taylorae@ornl.gov](mailto:taylorae@ornl.gov)

- [1] S. Boseggia, R. Springell, H. C. Walker, A. T. Boothroyd, D. Prabhakaran, D. Wermeille, L. Bouchenoire, S. P. Collins, and D. F. McMorrow, *Phys. Rev. B* **85**, 184432 (2012).
- [2] S. Boseggia, R. Springell, H. C. Walker, H. M. Rønnow, C. Rüegg, H. Okabe, M. Isobe, R. S. Perry, S. P. Collins, and D. F. McMorrow, *Phys. Rev. Lett.* **110**, 117207 (2013).
- [3] S. Calder, G.-X. Cao, S. Okamoto, J. W. Kim, V. R. Cooper, Z. Gai, B. C. Sales, M. D. Lumsden, D. Mandrus, and A. D. Christianson, *Phys. Rev. B* **89**, 081104 (2014).
- [4] J. Kim, D. Casa, M. H. Upton, T. Gog, Y.-J. Kim, J. F. Mitchell, M. van Veenendaal, M. Daghofer, J. van den Brink, G. Khaliullin, and B. J. Kim, *Phys. Rev. Lett.* **108**, 177003 (2012).
- [5] B. J. Kim, H. Jin, S. J. Moon, J.-Y. Kim, B.-G. Park, C. S. Leem, J. Yu, T. W. Noh, C. Kim, S.-J. Oh, J.-H. Park, V. Durairaj, G. Cao, and E. Rotenberg, *Phys. Rev. Lett.* **101**, 076402 (2008).
- [6] B. J. Kim, H. Ohsumi, T. Komesu, S. Sakai, T. Morita, H. Takagi, and T. Arima, *Science* **323**, 1329 (2009).
- [7] M. Moretti Sala, M. Rossi, S. Boseggia, J. Akimitsu, N. B. Brookes, M. Isobe, M. Minola, H. Okabe, H. M. Rønnow, L. Simonelli, D. F. McMorrow, and G. Monaco, *Phys. Rev. B* **89**, 121101 (2014).
- [8] B. F. Phelan, J. Krizan, W. Xie, Q. Gibson, and R. J. Cava, *Phys. Rev. B* **91**, 155117 (2015).
- [9] J. Chaloupka, G. Jackeli, and G. Khaliullin, *Phys. Rev. Lett.* **105**, 027204 (2010).
- [10] G. Jackeli and G. Khaliullin, *Phys. Rev. Lett.* **102**, 017205 (2009).
- [11] I. Kimchi and A. Vishwanath, *Phys. Rev. B* **89**, 014414 (2014).
- [12] W. Witczak-Krempa, G. Chen, Y. B. Kim, and L. Balents, *Annual Review of Condensed Matter Physics* **5**, 57 (2014).
- [13] K.-I. Kobayashi, T. Kimura, H. Sawada, K. Terakura, and Y. Tokura, *Nature* **395**, 677 (1998).
- [14] K.-I. Kobayashi, T. Kimura, Y. Tomioka, H. Sawada, K. Terakura, and Y. Tokura, *Phys. Rev. B* **59**, 11159 (1999).
- [15] H. L. Feng, M. Arai, Y. Matsushita, Y. Tsujimoto, Y. Guo, C. I. Sathish, X. Wang, Y.-H. Yuan, M. Tanaka, and K. Yamaura, *J. Am. Chem. Soc.* (2014).
- [16] R. Morrow, J. W. Freeland, and P. M. Woodward, *Inorg. Chem.* **53**, 7983 (2014).
- [17] R. Morrow, J. Yan, M. A. McGuire, J. W. Freeland, D. Haskell, and P. M. Woodward, *Phys. Rev. B* **92**, 094435 (2015).
- [18] A. A. Aczel, D. E. Bugaris, L. Li, J.-Q. Yan, C. de la Cruz, H.-C. zur Loye, and S. E. Nagler, *Phys. Rev. B* **87**, 014435 (2013).
- [19] T. Aharen, J. E. Greedan, F. Ning, T. Imai, V. Michaelis, S. Kroecker, H. Zhou, C. R. Wiebe, and L. M. D. Cran- swick, *Phys. Rev. B* **80**, 134423 (2009).
- [20] P. L. Bernardo, L. Ghivelder, H. S. Amorim, J. J. Neumeier, and S. Garcia, *arXiv:1509.04377* (2015).
- [21] J. P. Carlo, J. P. Clancy, K. Fritsch, C. A. Marjerrison, G. E. Granroth, J. E. Greedan, H. A. Dabkowska, and B. D. Gaulin, *Phys. Rev. B* **88**, 024418 (2013).
- [22] E. V. Kuz'min, S. G. Ovchinnikov, and D. J. Singh, *Phys. Rev. B* **68**, 024409 (2003).
- [23] E. Kermarrec, C. A. Marjerrison, C. M. Thompson, D. D. Maharaj, K. Levin, S. Kroecker, G. E. Granroth, R. Flacau, Z. Yamani, J. E. Greedan, and B. D. Gaulin, *Phys. Rev. B* **91**, 075133 (2015).
- [24] A. S. Erickson, S. Misra, G. J. Miller, R. R. Gupta, Z. Schlesinger, W. A. Harrison, J. M. Kim, and I. R. Fisher, *Phys. Rev. Lett.* **99**, 016404 (2007).
- [25] S. Gangopadhyay and W. E. Pickett, *Phys. Rev. B* **91**, 045133 (2015).
- [26] S. Middey, A. K. Nandy, S. K. Pandey, P. Mahadevan, and D. D. Sarma, *Phys. Rev. B* **86**, 104406 (2012).
- [27] H. Matsuura and K. Miyake, *J. Phys. Soc. Jpn.* **82**, 073703 (2013).
- [28] G. Chen and L. Balents, *Phys. Rev. B* **84**, 094420 (2011).
- [29] A. A. Aczel, P. J. Baker, D. E. Bugaris, J. Yeon, H.-C. zur Loye, T. Guidi, and D. T. Adroja, *Phys. Rev. Lett.* **112**, 117603 (2014).
- [30] G. J. Nilsen, C. M. Thompson, G. Ehlers, C. A. Marjerrison, and J. E. Greedan, *Phys. Rev. B* **91**, 054415 (2015).
- [31] A. E. Taylor, R. Morrow, D. J. Singh, S. Calder, M. D. Lumsden, P. M. Woodward, and A. D. Christianson, *Phys. Rev. B* **91**, 100406 (2015).
- [32] Y. Krockenberger, M. Reehuis, M. Tovar, K. Mogare, M. Jansen, and L. Alff, *Journal of Magnetism and Magnetic Materials* **310**, 1854 (2007).
- [33] Y. Krockenberger, K. Mogare, M. Reehuis, M. Tovar, M. Jansen, G. Vaitheeswaran, V. Kanchana, F. Bultmark, A. Delin, F. Wilhelm, A. Rogalev, A. Winkler, and L. Alff, *Phys. Rev. B* **75**, 020404 (2007).
- [34] O. N. Meetei, O. Erten, M. Randeria, N. Trivedi, and P. Woodward, *Phys. Rev. Lett.* **110**, 087203 (2013).
- [35] A. K. Paul, A. Sarapulova, P. Adler, M. Reehuis, S. Kanungo, D. Mikhailova, W. Schnelle, Z. Hu, C. Kuo, V. Siruguri, S. Rayaprol, Y. Soo, B. Yan, C. Felser, L. Hao Tjeng, and M. Jansen, *Z. anorg. allg. Chem.* **641**, 197 (2015).
- [36] Y. Yuan, H. L. Feng, M. P. Ghimire, Y. Matsushita, Y. Tsujimoto, J. He, M. Tanaka, Y. Katsuya, and K. Ya-

- maura, *Inorg. Chem.* (2015), 10.1021/ic503086a.
- [37] J.-H. Choy, D.-K. Kim, and J.-Y. Kim, *Solid State Ionics* **108**, 159 (1998).
  - [38] G. E. Granroth, A. I. Kolesnikov, T. E. Sherline, J. P. Clancy, K. A. Ross, J. P. C. Ruff, B. D. Gaulin, and S. E. Nagler, *J. Phys.: Conf. Ser.* **251**, 012058 (2010).
  - [39] Supplementary material includes additional INS data and spin-wave model calculations.
  - [40] Assuming a g-factor of 2, which is reasonable since the ratio of spin to orbital moments is  $\sim 15$  according to DFT [31].
  - [41] S. Toth and B. Lake, *J. Phys.: Condens. Matter* **27**, 166002 (2015).
  - [42] Space group  $Fm\bar{3}m$  has inversion symmetry on the Os site,  $P2_1/n$  does not.
  - [43] D. I. Khomskii, *Transition Metal Compounds*, 1st ed. (Cambridge University Press, Cambridge, 2014).
  - [44] S. Kanungo, B. Yan, M. Jansen, and C. Felser, *Phys. Rev. B* **89**, 214414 (2014).
  - [45] Y. S. Hou, H. J. Xiang, and X. G. Gong, *Scientific Reports* **5**, 13159 (2015).
  - [46] J. Wang, N. Zu, X. Hao, Y. Xu, Z. Li, Z. Wu, and F. Gao, *Physica Status Solidi (RRL)* **08**, 776 (2014).
  - [47] S. Vasala and M. Karppinen, *Progress in Solid State Chemistry* **43**, 1 (2015).